Friction **11**(6): 1027–1039 (2023)
https://doi.org/10.1007/s40544-022-0644-3
ISSN 2223-7690
CN 10-1237/TH
RESEARCH ARTICLE

Is there more than one stickiness criterion?

Anle WANG[1], **Martin H. MÜSER**[1,2,*]

[1] *Department of Material Science and Engineering, Saarland University, Saarbrücken 66123, Germany*

[2] *INM–Leibniz Institute for New Materials, Saarbrücken 66123, Germany*

Received: 18 February 2022 / Revised: 08 April 2022 / Accepted: 29 April 2022

Abstract: Adhesion between an elastic body and a smooth, rigid substrate can lead to large tensile stresses between them. However, most macroscopic objects are microscopically rough, which strongly suppresses adhesion. A fierce debate has unfolded recently as to whether local or global parameters determine the crossover between small and large adhesion. Here, we report simulations revealing that the dependence of the pull-off force F_n on the surface energy γ does not only have two regimes of high and low adhesion but up to four regimes. They are related to contacts, which at the moment of rupture consist of (i) the last individual Hertzian-shaped contact, in which is linear in γ, (ii) a last meso-scale, individual patches with super-linear scaling, (iii) many isolated contact patches with extremely strong scaling, and (iv) a dominating largest contact patch, for which the pull-off stress is no longer negligible compared to the maximum, microscopic pull-off stress. Regime (iii) can be seen as a transition domain. It is located near the point where the surface energy is half the elastic energy per unit area in conformal contact. A criterion for the transition between regimes (i) and (ii) appears difficult to grasp.

Keywords: adhesion; pull-off force; rough contact; stickiness

1 Introduction

When two solids come into contact, attraction due to van der Waals interaction is unavoidable. If their surfaces were perfectly smooth, maximum tensile forces between them could be crudely estimated through the ratio of surface energy γ, which is typically of order 50 mJ/m², and their interaction range, ρ which is roughly 5 Å. However, we all know that lifting off an object with an area of $A = 1$ cm² does not necessitate a force anywhere near $A\gamma/\rho = 10,000$ N. The established reason for the failure of our crude calculation is that the elastic energy needed to conform two surfaces to each other generally exceeds the surface energy gained during microscopic contact formation by orders of magnitude [1–6]. This is why only a small fraction of the nominal contact is in microscopic contact when a zero or tensile normal load is applied. As a consequence, the pull-off stress (averaged over a domain large compared to atoms but small compared to macroscopic dimensions) must be small compared to maximum local tensions, unless, the surfaces are very smooth and/or the solids are extremely compliant.

The elastic energy needed to conform two surfaces to each other, v_{fce}, is dominated by contributions from large-wavelength height undulation when the Hurst roughness exponent H lies in the typical range of $0.5 < H < 1$ [2, 4–7]. Adding roughness at small wavelengths then barely increases v_{fce} although it does increase the local mean-square gradient g^2 and even more so the local mean-square curvature κ^2, see also Eq. (A2). It thus came as a surprise when Pastewka and Robbins [8] proposed a criterion for macroscopic adhesion less than a decade ago that depends only on local parameters. Their theory, which received much skepticism [2, 4–7, 9, 10], is based on the question above what surface energy the area–load

* Corresponding author: Martin H. MÜSER, E-mail: martin.mueser@mx.uni-saarland.de

Nomenclature

ΔW	dissipation energy in a loading/unloading cycle	H	Hurst exponent
Δa	linear size of a mesh element	R_C	characteristic radius curvature of rough substrate
α	Johnson parameter		
γ	surface energy	W	work of adhesion
$\tilde{\gamma}$	reduced surface energy	a_r	relative contact area
$\tilde{\gamma}_t$	reduced surface energy at transition	g	mean gap or interfacial separation
$\tilde{\gamma}_{loc}$	local reduced surface energy	g^2	mean square gradient
κ^2	mean square curvature	$\tilde{h}(q)$	Fourier transform of the substrate height
λ_s	short wavelength cut-off	$\overline{h}^2$	mean square height
λ_r	roll-off wavelength	h_{rms}	root-mean-square height
μ_T	Tabor parameter	p	external normal pressure
ρ	characteristic range of adhesion	p^*	reduced contact pressure
σ	pull-off stress	q_0	smallest non-zero wavelength in the system
A	nominal contact area	r_d	domain size ratio
$C(q)$	height spectra of indenter	r_f	fractal ratio
E^*	contact modulus	v_{ela}	elastic energy in true contact
F_p	pull-off force	v_{fce}	elastic energy in full contact
F_{max}	maximum characteristic tensile force		

relation seizes to be (approximately) linear at small reduced pressures $p^* \equiv p/(E^* g)$, where p is the nominal contact pressure. At that point, a non-negligible relative contact area forms at zero load so that a perceivable force might be needed to separate the surfaces.

Simulations, which revealed that adding roughness at small wavelengths in fact does not alter pull-off forces, apparently rebutted the necessity for a local stickiness criterion [4, 9]. However, such calculations are not particularly telling when the range of adhesion exceeds the amplitude of the added roughness. In fact, an analysis of the gap distribution function of adhesive, randomly rough, adhesive surfaces revealed that the gap distribution function lost its asymptotic $g^{-1/3}$ scaling at small gaps g near the point, where local stickiness criteria predict the onset of stickiness [11]. In addition, simulations using short-range adhesion down to the smallest scale indicated a transition between sticky and non-sticky, which apparently supported the Pastewka Robbins criterion [12]. However, this time, the limited system size can be argued to have led to false conclusions. Thus, the validity of or even the necessity for a local stickiness criterion remains an open issue.

The above-presented argument raised against the necessity of local stickiness criteria starts from the large scale and investigates what happens if more roughness is added at small wavelengths. However, this procedure needs to be inverted when investigating if the contact formation of a single mesoscale contact patch is hysteretic, or, sticky. Here, we call a contact patch mesoscale when it extends over a connected domain large enough to include saddle points and maxima of the undeformed gaps.

The dynamics of contact formation and rupture of such an (isolated) contact patch, as well as the tensile load it can carry, obviously depend on the local geometry but are unaffected by the height profile of the substrate far away from it, as is demonstrated in Fig. 1. The roughness unfolding to the left and to the right of the shown domain does not impact the load-bearing ability of the central contact patch as long as that additional domain makes no contact with the elastic body. In other words, when keeping the properties of the height spectrum at short wavelengths, thus fixing g, increasing the ratio of short wavelength cutoff and roll-off wavelength λ_s/λ_r —both implicitly

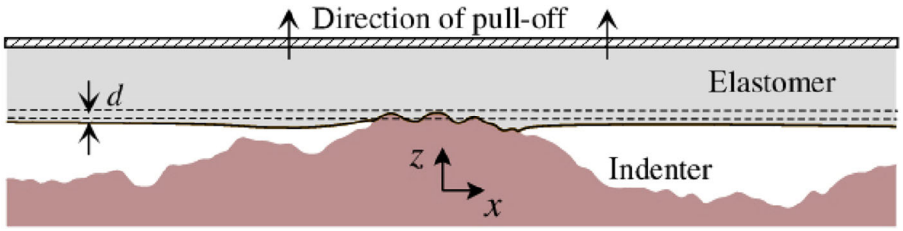

Fig. 1 Cross-section of an adhesive elastic body, which is pulled off a rigid, self-affine substrate. The interference d is the difference between the elastic body's bottom-surface center-of-mass and the indenter's highest point. The shown cross-section contains the highest point of our default configuration. The shown cross-section is 10% of a cut through the square simulation cell.

defined further below in Eq. (1) through their corresponding wave numbers—would reduce the number density of the mesoscale contact patches and thus the total load they can carry but not their individual stickiness. Thus, it seems as though asking whether individual contact patches are sticky and to what degree this can be observed in a macroscopic experiment are two separate issues, which we address in this work using computer simulations.

2 Model

Our model is similar to that used in previous numerical studies [12, 13]. Specifically, a rigid substrate and an elastic body interact through a Morse potential for which the areal interaction energy density reads $v(g)=\gamma(\mathrm{e}^{-2g/\rho}-2\mathrm{e}^{-g/\rho})$. Here, γ is the energy gained when making microscopic contact, g is the gap between the surfaces, a negative gap indicating an overlap, and ρ is the interaction range. The elastic energy density is given by $v_{\mathrm{ela}}=(E^*/4)\sum_q q|\tilde{u}(q)|^2$, where $\tilde{u}(q)=\frac{1}{A}\int \mathrm{d}^2 r \mathrm{e}^{-\mathrm{i}\boldsymbol{q}\cdot\boldsymbol{r}}u(r)$ is the Fourier transform of the periodically repeated displacement field $u(\boldsymbol{r})$ of the elastic body defined in the xy-plane. The domain is a square with an area of $A=\mathcal{L}^2$, so that the smallest non-zero wavenumber fitting into it is $q_0=2\pi/\mathcal{L}$.

The Fourier transform of the substrate height, $\tilde{h}(\boldsymbol{q})$, is given by default by

$$h(\boldsymbol{q})=\sqrt{\frac{C(q_r)}{A}}\mathrm{e}^{\mathrm{i}2\pi X(\boldsymbol{q})}\times\begin{cases}1 & \text{for } q_0\le q<q_r\\ \left(\dfrac{q_0}{q}\right)^{1+H} & \text{for } q_r\le q\le q_s\end{cases} \quad (1)$$

and zero else, reflecting real height spectra, $C(q)\equiv A|\tilde{h}(\boldsymbol{q})|^2$, for a wide variety of surfaces [14]. Here, h_0 is a constant of unit length, $X(q)$ a uniform random variable on (0, 1), and $q_{\mathrm{r,s}}=2\pi/\lambda_{\mathrm{r,s}}$. Important numbers to be deduced from Eq. (1) are the mean-square (ms) height h^2, ms height gradient g^2, ms height curvature κ^2, and the full-contact elastic energy v_{fce}. The dependencies of these quantities on the variables defining the height spectrum are compiled in the Appendix. Note that the exponent $1+H$ in Eq. (1) must be replaced with $0.5+H$ for line indenters.

Simulations were run using a house-written Green's function molecular dynamics code [15] using mass-weighting in combination with the fast-internal-relaxation-engine (FIRE) optimizer, as described previously [16]. The elastic body and rigid rough substrate are brought into contact at zero external stress. Only one set of simulations considers different preloads. They are reported in the last figure of this work. Retraction was achieved through a ramp, in which the elastic body's center-of-mass, $\tilde{u}(q=0)$, was changed quasi-continuously from one value to the next within 200 time steps by moving $\tilde{u}(q=0)$ in steps of 0.1% of the root-mean-square height, which translates to 2% of the interaction range at a Tabor parameter of $\mu_{\mathrm{T}}=1$. This was then followed by a relaxation of 600 time steps at fixed $\tilde{u}(q=0)$. Using this procedure, the surface moves in a quasi-static fashion so that viscoelastic and inertial effects are small. Any hysteresis reported in the results section therefore relates to adiabatic processes. In real experiments [17], the work of adhesion and the energy hysteresis would be generally larger, in particular when allowing the system to relax between compression and decompression.

Throughout this work, all (dimensionless) parameters defining the model were varied, except for the Hurst exponent H, which was kept at $H=0.8$, because this

a rather generic value. The two remaining dimensionless parameters defining the height spectrum are "domain-size ratio" $r_d = \mathcal{L}/\lambda_d = 4$ and "fractal ratio" $r_f = \lambda_r/\lambda_s = 64$. Moreover, the default (local) Tabor parameter defined as $\mu_T \equiv \rho^{-1} R_c^{1/3} (\gamma/E^*)^{2/3}$ was set to $\mu_T = 1$. The reduced surface energy $\tilde{\gamma} \equiv \gamma/v_{fce}$ was varied over several orders of magnitude for each system.

When relating our model to real systems, γ should be of order 50 mJ/m² and λ_s around one nanometer, or, if we assumed our smallest mesh to be already slightly coarse, λ_s would be a few ten nanometers, in which case γ would need to be reduced by the elastic energy per unit area required to make contact at the scales below the mesh size Δa. Thus, when changing $\tilde{\gamma}$, we don't have a mind a change of the surface energy itself, but rather of the other parameters affecting γ, E_0^* or the height spectrum, because these parameters tend to vary much more from one experiment to the next than the surface energy. In this sense, when calling adhesion small, we don't mean to say a small value of the real surface energy but the reduced surface energy. In addition, we assume the length of the simulation cell to be small compared to the normal dimension of the elastic body so that macroscopic peeling or confinement effects can be neglected. In many cases, it would be appropriate to consider our entire simulation cell to represent a single element in finite-element method based simulations [18–20] of technical systems.

The discretization of the elastic body was set to $\Delta a = \lambda_s/16$. Even for the largest values of γ considered here, this choice turned out sufficient to avoid lattice trapping, i.e., contact hysteresis associated with individual degrees of freedom, which are mesh elements in our case. In the absence of lattice trapping, reducing Δa at fixed range of interaction alters the values for our quantities of interest only by a few percent so that trends remain unchanged. The default system size was $4{,}096 \times 4{,}096$. Several hundred if not thousand simulations had to be run in total, each one being fairly long with thousands of steps forming the stepped ramp, each step in a ramp necessitating 800 time steps. Due to this large computational burden, we did not attempt to reduce the minor systematic discretization errors, which would have required us to quadruple the number of Green's function molecular dynamics (GFMD) elements. Instead, we found it more important to reduce statistical uncertainties by averaging over a few, usually five random realizations. In fact, many more simulations were conducted than those summarized here. However, it took us some time to detect coherent trends and to represent them such that they are not hidden by data scatter.

3 Results

To set the stage for the analysis of how different dimensionless parameters affect the pull-off force in adhesive systems, we first present results on an individual random realization for our default parameter set. This choice makes the ratio of the range of interaction used in the Morse potential and the root-mean-square height take the values $\sigma/h_{rms} = 0.125$ for $\tilde{\gamma} = 1$ and $\sigma/h_{rms} = 0.0268$ for $\tilde{\gamma} = 0.1$. Given that the difference between the highest and the lowest point is roughly $4h$, the range of interaction—using a fixed ratio of mesh size and λ_s—turns out approximately 3% of $|\max(h) - \min(h)|$ even at the high end of investigated surface energies.

Figure 2(a) reveals three obvious regimes for the dependence of the pull-off force on the reduced surface energy $\tilde{\gamma}$: A large and a small pull-off force regime at $\tilde{\gamma} \gtrsim 0.8$ and $\tilde{\gamma} \lesssim 0.3$, respectively. They are separated by a narrow cross-over regime near $\tilde{\gamma} \approx 0.5$. Averaging similar curves over several random realizations clearly broadens the cross-over regime. However, for any investigated individual system, we did not find the cross-over regime to be significantly larger than the one reported in Fig. 2(a), even when increasing the system size or reducing the short-wavelength cutoff by a factor of four while keeping the roll-off wavelength fixed. This claim will be substantiated further below.

To explore the correlation between relative contact area and stickiness, Fig. 2(b) reports the relative contact area $a_r(\tilde{\gamma}, F = 0)$ as obtained under zero load (full squares) and right before snap off, $a_r(\tilde{\gamma}, F_p^-)$ during the retraction from a zero-load configuration (open squares). Here, we only count surface points under compressive stress toward true contact. Interestingly, the scaling of $a_r(\tilde{\gamma}, 0)$ appears to level off with increasing $\tilde{\gamma}$ before it starts picking up again,

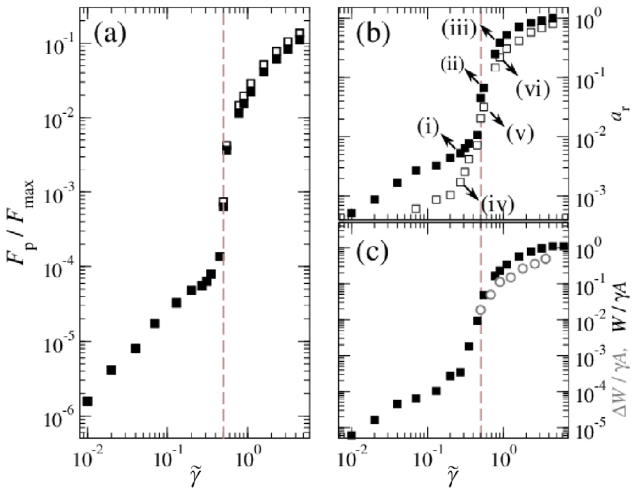

Fig. 2 (a) Pull-off force F_p, (b) relative contact area a_r, and (c) work of adhesion W (closed squares) as well as energy hysteresis ΔW (grey open circles) for one realization of the default surface. Open symbols in panel (a) relate to contacts in which the elastic body was retracted when the normal load reached zero for the first time, while closed symbols relate to earlier retractions right after the tensile stress was maximal. Both data sets overlap for $\gamma < 0.5$. Closed and open symbols in panel (b) show a_r at zero load and just before snap-off, respectively. Variables were normalized as follows: F_p is expressed in units of F_{max}, which is the maximum tensile stress of the cohesive zone model times the nominal contact area, while γ is divided by the elastic, full-contact, areal energy density v_{fce}. Finally, W and ΔW are normalized by γ times the nominal contact area A.

something we found to be the rule at relatively small λ_r / λ_s ratios rather than a peculiarity of this individual random realization. The data points labeled (i) and (iv) in Fig. 2(b) are the last ones for which the contact at zero load and at snap-off consist of a single patch, see Fig. 3, where the contact stresses are shown according to the numerals (i)–(vi) used in Fig. 2(b).

The transition between sticky and non-sticky also becomes apparent in the work of separation W, which is the work done to separate the two surfaces from a zero load configuration, and most prominently in the dissipated energy ΔW that is lost in a closed cycle, in which the surfaces are first brought quasi-statically into zero-load contact and then separated quasi-statically again. In Fig. 2(c), both quantities change substantially near $\gamma = 0.5$ where depinning force F_p and non-contact area $1 - a_r$ also have a steep dependence on adhesion. Due to the small hysteresis that occurs for $\mu_T = 1$, single-asperity contacts [10, 21] and the ensuing difficulty to compute accurate numbers, we abstained from reporting our estimates for ΔW at $\tilde{\gamma} < 0.5$. However, ΔW drops at least by three decades when the hysteresis is related to the snap off of an individual asperity compared to the lowest investigated value of $\tilde{\gamma}$ at which we find more than one contact patch at snap-off in our default configuration.

The cross-over between the sticky, large-pull-off-force regime and the non-sticky, small-pull-off-force regime correlates with qualitative changes in the contact topography, which can be deduced from selected zero-load and pull-off-force stress fields shown in Fig. 3. They reveal a cross-over from a close-to-percolating contact to a single-asperity contact and a reduction of relative, repulsive contact area from 0.71 to 0.0075 when the surface energy is merely reduced by a factor of approximately three. To achieve a similar change for a non-adhesive contact under a compressive load L, L needs to be reduced from $L \approx 0.44 E^* / g$ by a factor slightly exceeding 100 for the given system [22]. Here, we call the system to be "close-to-percolating" when it is possible to identify a path through it from one side to the opposite side such that the (linear dimension of the) visited non-contact domains are never larger than the larger of two adjacent contact patches that need to be visited on the path.

In real systems, the "fractal ratio" r_f is much larger than the ones that can be currently realized in simulations. To nevertheless ascertain if the reported trends remain robust under varying fractal ratios, we added $r_f = 32$ and $r_f = 128$ to our analysis, while keeping all other dimensionless parameters used in the problem definition constant. In addition, we considered $r_f = 512$ for which the domain-size ratio r_d was reduced to unity. All cases were averaged over five independent random realizations, which smears out the cross-over regime, since its location varies somewhat from one random realization to the next. Geometric means were chosen, because they reduce the effect of statistical outliers compared to arithmetic or harmonic averages.

Figure 4(a) reveals that increasing r_f makes the transition between single to many-asperity contacts move to slightly larger $\tilde{\gamma}$. Coming from large $\tilde{\gamma}$, the drop in depinning force and—even more clearly—in the work of adhesion and its hysteresis still occur at

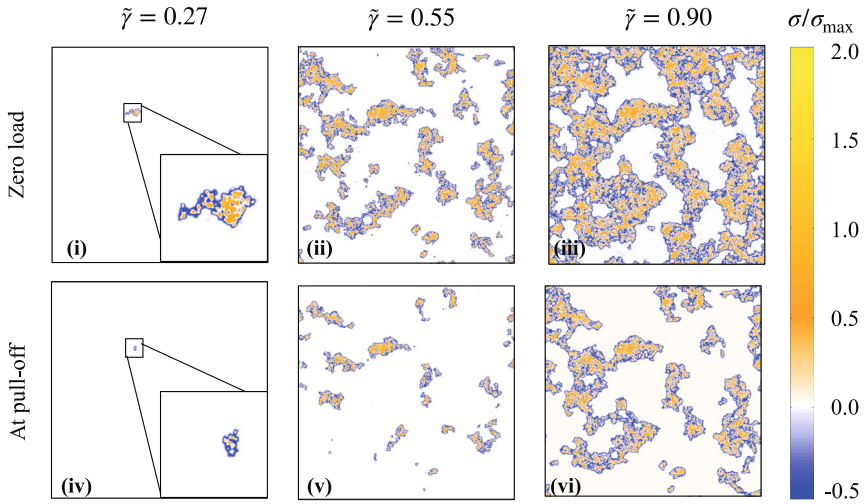

Fig. 3 Stress fields of configuration at zero-load (top row) and right before snap-off (bottom row) for reduced surface energies $\tilde{\gamma}$ at the large-$\tilde{\gamma}$ end of the non-sticky regime (left column, $\tilde{\gamma} = 0.27$), in the center of the cross-over regime (center column, $\tilde{\gamma} = 0.55$), and at the low-$\tilde{\gamma}$ end of the sticky regime (right column, $\tilde{\gamma} = 0.90$). The labels (i)–(vi) correspond to those used in Fig. 2(b).

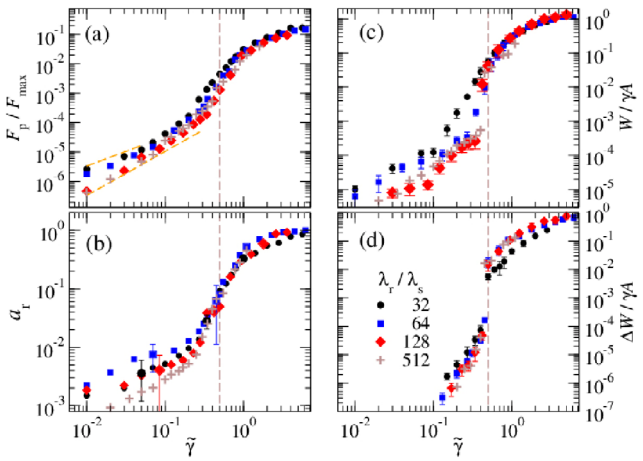

Fig. 4 Same quantities as in Fig. 2. This time, different ratios $r_f = \lambda_r/\lambda_s$ are considered and results averaged geometrically over five independent configurations. Moreover, only zero-load relative contact areas are shown. In addition, the work of separation and its hysteresis are represented in two separate panels, i.e., in (c) and (d), respectively. Dashed lines are drawn to guide the eye. Circles, squares, diamonds, and plus symbols represent the data sets for $r_f = 32, 64, 128,$ and 512, respectively.

the latest near $\tilde{\gamma} = 1/2$. In addition, subtle indications for a change of scaling can be found in the single-asperity-contact regime. Specifically, Fig. 4 reveals (a) a slight crossover in the $F_p(\gamma)$ scaling for $r_f = 512$ near $\tilde{\gamma}_{1c} = 0.1$ and (b) in the $W(\tilde{\gamma})$ scaling for $r_f = 128$, again near $\tilde{\gamma} = 0.1$. Inside the single-asperity regime, the values of $\tilde{\gamma}$, where the $a_r(\tilde{\gamma})$ scaling crosses over from Hertzian to a meso-scale contact-patch scaling, are difficult to ascertain. For the smallest r_f, the increase of a_r at pull off with r_f even seems to level off at the large -$\tilde{\gamma}$ end of the single-asperity regime, while no clear changes in scaling are detectable for the largest studied value of r_f. For a recent analysis of how the contact area scales at fixed adhesion with a changing compressive load, we refer the reader to a recent study by Salehani et al. [23].

Unfortunately, the results presented in Fig. 4 do not provide fully conclusive information on the correctness of local stickiness criteria [8, 12]. They are based on a dimensionless surface energy, $\gamma_{loc} \equiv f(\mu_T)\gamma/(E^* R_c g^3)$, which depends only on local parameters, i.e., on the microscopic surface energy, the inverse characteristic surface curvature R_c, and a function of the Tabor parameter, $f(\mu_T)$. Neither, the scaling nor the function $f(\mu_T)$ were stated explicitly in the original literature [8]. However, for large μ_T, a power law dependence from the arguments presented in the original literature were deduced [12] according to which $\mu_T \propto \{\gamma/(E^* R_c g^3)\}^{7/3}$ with a prefactor of order unity. Using this dependence, we find $\gamma_{1c}(r_f = 128) \approx 0.235$ and $\gamma_{1c}(r_f = 512) \approx 0.112$ when $\gamma_{loc} = 1$ in our model, i.e., at the point where the local stickiness criterion predicts a transition between sticky and non-sticky. These numerical values are on par with the simulation results. Yet, the data do not allow us to confirm or to reject the correctness of the hypothesis that $\tilde{\gamma}_{1c}$ decreases with r_f when the Tabor parameter remains constant. Nonetheless, it seems clear that the sudden, drastic

increases of the pull-off force, work of adhesion, and its hysteresis coming from small $\tilde{\gamma}$ are related to the transition from single to multi-asperity contacts rather than to a cross-over in scaling of individual contact patches or to a dramatic increase of the relative contact area with adhesion.

We also analyzed the effect that the system size has on the scaling behavior within the various regimes and the locations separating them. To this end, we varied r_d from $r_d = 2$ to $r_d = 8$ while keeping the fractal ratio and the Tabor parameter constant. Figure 5 shows results of an individual surface realization rather than averages so that the sharpness of transitions between different scaling domains does not get smeared out through averaging. The individual realization was chosen to be the one for which $\tilde{\gamma}$ took the median value for the transition between the single and the many-asperity regime. Coming from large surface energies, no significant dependence on the surface energy on all measured quantities is observed down to a value of $\tilde{\gamma} \approx 1$, below which small systems are no longer self averaging. The transition from the many to single-asperity domain occurs again at $\tilde{\gamma}_t \approx 1/2$ in all cases. A marginal reduction, supposedly irrelevant in practice, is observed in $\tilde{\gamma}_t$ with increasing r_d. In contrast, all computed quantities reveal a clearly noticeable size dependence in the one-asperity regime. Interestingly, the pull-off force and relative contact area do not scale with $1/r_d^2$, which would happen if the (local) geometric features of the highest asperities and thus last asperity in contact were independent of r_d. Unraveling the nature for this correlation, which falls in the domain of extreme-event statistics, is beyond the scope of this work. It would be a similarly non-trivial exercise to ascertain the expected height difference between the highest and second-highest peak for a given spectrum. Brute-force computing appears to be the only option to get statistics.

The last varied dimensionless number is the Tabor parameter, see Fig. 6. It reveals an intricate dependence of the quantities of interest on μ_T, in particular with respect to long-range adhesion. First, the transition between single and many-asperities contacts is no longer sharp at small μ_T. Nonetheless, all computed properties keep changing their functional dependence on $\tilde{\gamma}$ around $\tilde{\gamma} = 0.5$, which, of course, will seize to be true in the (irrelevant) case of the interaction range being no longer small compared to the root-mean-square roughness. Second, the pull-off force, F_p, relative to its theoretically maximum value for flat contacts, F_{max}, is increased noticeably for $\tilde{\gamma} < 1$ as adhesion becomes long ranged. However, the absolute value of F_p is generally reduced compared to short-range adhesion, because F_{max} decreases with increasing interaction range. Yet, in the usual single-to-many-asperity-contact transition regime ($\tilde{\gamma} \approx 0.5$) even absolute values of F_p can be relatively high for long-ranged adhesion, since the surfaces can "see" many asperities in addition to the highest. Third, the energy hysteresis is reduced by many orders of

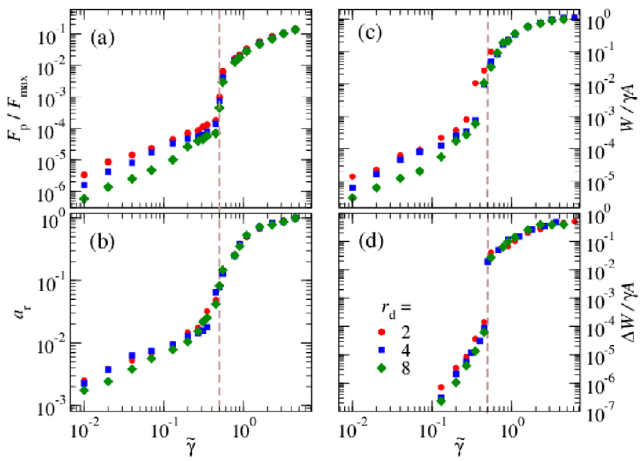

Fig. 5 Same quantities as in Fig. 4. This time, different ratios $r_d = \mathcal{L}/\lambda_d$ are considered with fixed $r_f = 64$. Here only one calculation is shown.

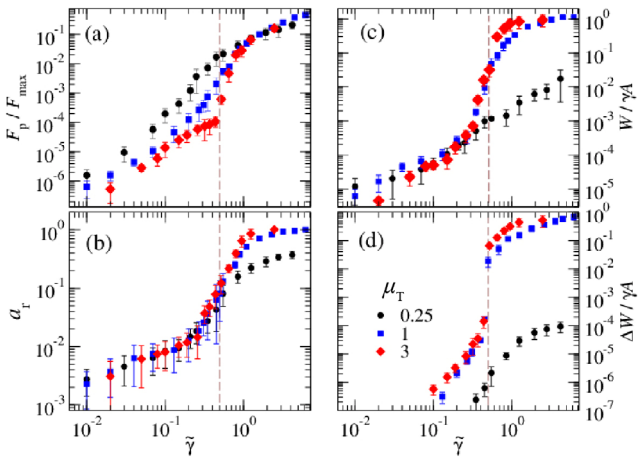

Fig. 6 Same quantities as in Fig. 4. Here, different Tabor parameter μ_T are considered with fixed $r_f = 64$ and $r_d = 4$.

magnitudes at small μ_T, while the work of adhesion and the relative contact area at small $\tilde{\gamma}$ do not seem to be sensitive to the range of adhesion, a phenomenon known quite well from single-asperity indenters. In addition, for large μ_T, the data collapses less well on a master curve, when varying γ_T than when varying r_s or r_d while keeping the other dimensionless variables describing the height spectrum fixed.

To further elucidate, amongst other things, the quasi-discontinuous change in the work of adhesion with surface energy, Fig. 7 shows load-displacement relations for various systems with reduced surface energies being $\tilde{\gamma} = 0.45$ times factors between roughly 2/5 and 5/2. The studied models include two "regular" two-dimensional contacts, both with Hurst exponent $H = 0.8$ and (a) $r_d = 5$ and $r_f = 102.4$, (b) $r_d = 1$ and $r_f = 512$ as well as a $H = 0.8$ line contact with (c) $r_d = 32$ and $r_f = 512$, and finally (d) a two-dimensional contact, in which the surface topography has only a single wave length, $r_d = r_f = 1$, and 90° rotational symmetry, similar to that of a square lattice. Specifically, the indenter profile (d) was defined as $h(x,y)/h_0 = -2 + \cos(q_0 x) + \cos(q_0 y)$ and $h_0 = 2h_{rms}$.

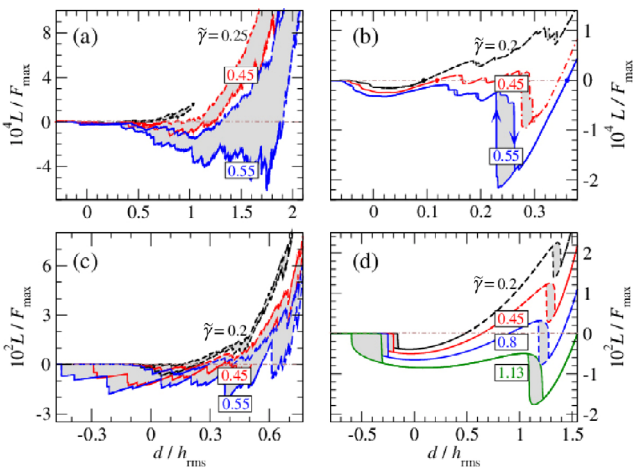

Fig. 7 Reduced compressive force, or, load L/F_{max}, as a function of the dimensionless interference d/h_{rms} in approach and retraction for different reduced surface energies $\tilde{\gamma}$ and different indenters. Their dimensionless numbers other than $H = 0.8$ are (a) $D = 2$, $r_d = 5$, $r_f = 102.4$, (b) $D = 2$, $r_d = 1$, $r_f = 512$, (c) $D = 1$, $r_d = 32$, $r_f = 512$, and (d) $D = 2$, $r_d = 1$, $r_f = 1$. Circles in (b) indicate the point of reaching zero load on approach for the first time. Dashed lines indicate a compression/decompression (c/d) cycle, for which the motion is returned after zero load is first reached. These point are indicated with a solid circle. Grey areas relate to dissipated energy.

At large surface energy, e.g., at $\tilde{\gamma} = 0.55$ for randomly rough systems (a–c) and $\tilde{\gamma} = 1.13$ for the single-sinusoidal indenter (d), the hystersis occurs (predominantly) at a negative stress. This moves toward a zero-stress hysteresis as the reduced surface energy decreases. Once reduced surface energies are small, i.e., at $\tilde{\gamma} \le 0.25$, the energy hysteresis is much reduced and predominantly located at compressive stresses.

The just-discussed behavior accounts for the quasi-discontinuous change of the various stickiness criteria with surface energy. For example, the $\tilde{\gamma} = 0.45$ and $\tilde{\gamma} = 0.55$ approach curves in panel (b) look similar up to the interference① d^*_{low}, where the contact with the slightly lower adhesion reaches zero, at which point the displacement direction is reverted. Upon retraction, a tiny hysteresis, which cannot be resolved with the used line width, ensues for the less-adhesive system. For the slightly greater surface energy, the first instance of zero load occurs at a much greater interference, since the tensile load increases again after it had almost reached the value of zero. Thus, a small change in γ can substantially change what fraction of a load-displacement curve is sampled when reverting the compression at the first zero-load occurrence. This leads to a substantial change of all stickiness criteria, which would have also occurred if the compression had been reverted at a slightly positive load, which could be, for example, the gravitational load of the indenter. However, the largest relative discontinuity occurs in the energy hysteresis.

Panels (b) and (d) in Fig. 7 also reveal that the hysteresis is relatively well localized when the system size (or the domain over which the stress-strain relation is coarse-grained) does not exceed the roll-off wavelength, in which case the hysteresis only extends over a range that is clearly less than 0.1 times the root-mean-square height, as is the case for the investigated single-sinusoidal roughness. This region becomes substantially larger as the roll-off domain, i.e., the ratio $\mathcal{L}/\lambda_r$ increases.

Qualitatively, panels (b) and (d) in Fig. 7 look similar in that the load-displacement curves, $L(d)$, show two clear minima, which are located at medium and large interferences. They can be readily interpreted for the

① The interference is defined in the caption of Fig. 1.

single-sinusoidal roughness (d), as contact formation of the highest peak at small interference and of the saddle point at intermediate interference. A similar interpretation can be said to hold for the randomly rough contact of model (b), even if quite a few small-scale instabilities become apparent. The reason why (b) shows no hysteresis regarding the highest asperity is that the local Tabor parameter is $\mu_T = 1$, while interactions in the single-sinusoidal contact were shorter ranged and characterized with $\mu_T = 7$. The surface undulations becoming unstable at an increased interference $d / h_{rms} \approx 0.25$ for indenter (b) are related to relatively coarse scales, which is why a scale-dependent Tabor parameter would clearly exceed unity at the relevant length scale.

A saddle-point instability, as that observed in model (d) of Ref. [24], or, in related single-wavelength, two-dimensional (SW2D) indenters with 60° rotational symmetry, does not exist in single-wavelength line contacts (SWLCs) [25]. Obviously, line contacts do not even have saddle-points, which in a leakage context could also be called constrictions, since they cannot have profiles that are maximal along one direction and minimal in the (non-existing) orthogonal, interfacial direction. To investigate if this qualitative difference between one- and two-dimensional interfaces matters beyond single-wavelength roughness also for randomly rough surfaces, we complemented our simulations with one-dimensional (1D) randomly rough indenters.

A comparison between 1D and 2D randomly rough indenters both having a non-negligible roll-off domain, as well as identical dimensionless numbers $H = 0.8$, $r_f = 102.4$, and $\mu_T = 1$, reveal both similarities and discrepancies, see Figs. 7(a) and 7(c). Before discussing them, we wish to clarify that a 1D indenter with $r_d = 5$, which is the value used for the 2D system, yields similar results as those shown for $r_d = 32$ but has greater data scatter, which is why we kept the latter for panel (d). A similarity between randomly rough 1D and 2D is the value where stickiness starts to pick up upon increasing adhesion, which in both cases is near $\tilde{\gamma} = 0.5$. However, the point of rupture after decompression occurs at distinctly more negative interferences for the 1D than for the 2D indenter. More importantly, the reduced pull-off load is almost two orders of magnitude larger in 1D than in 2D. Similarly, the relative contact area at pull off is much larger in 1D than in 2D, this time by a factor of approximately ten. These results are surprising given that the differential $C(q)\mathrm{d}^2q$ is identical for 1D and 2D surfaces on the self-affine branch as long as both have similar values H and similar cut-off and roll-off wavelengths.

Interestingly, Johnson [26] found similar results for a one-dimensional, single-sinusoidal surface as we do for random roughness. Specifically, he found jump into complete contact when his parameter, $\alpha := \left(\frac{4\gamma}{q_0 \pi h_0^2 E^*}\right)^{1/2}$, satisfied $\alpha \geq \alpha_c \approx 0.6$. This condition can be recast as $\tilde{\gamma} > \pi\alpha_c^2 \approx 1.1$, which differs from our results only by a factor of two, if an almost percolating contact of a rough surface is associated with a full contact in Johnson's model.

4 Conclusions

In this work, we demonstrated that possible quantitative measures for stickiness, which are pull-off force, work of adhesion, and energy hysteresis, are most sensitive to the adhesion for simple, randomly rough surfaces, when the elastic energy needed to make full contact is roughly half the adhesive energy gained in full contact, whereby we corroborate previous works [2, 4, 6, 7, 9, 17, 27–29] emphasizing the importance of a global energy analysis for the assessment of stickiness over purely local stickiness criteria [8, 12]. Here, we say the sensitivity to be largest, when the relative change of the pull-off force with the relative change of the reduced surface energy is maximal. The precise value of this criterion might have to be altered for surfaces with correlation, in particular those having deep dimples. The relevant elastic energy density, which the surface energy would have to be compared to, might then be better defined relative to the elastic energy needed to create a percolating contact, e.g., the energy needed to create roughly 40% relative contact area [30, 31]. Once a contact percolates or is close to percolation, large, load-bearing contact patches can no longer be easily peeled off, at which point the macroscopic pull-off force starts to be sensitive to the maximum stress of the microscopically

valid traction law. Once a contact is far away from percolating at zero external force, it seems as though the adhesive pull-off is determined by one last asperity contact, or, depending on boundary conditions, e.g., when surfaces can tilt, by three last contact points. This speculation is supported by recent observations on the critical angular velocity of spinning asteroid, where non-gravitational, attractive forces between the rubble particles were found to not increase with their size [32]. Nonetheless, local stickiness criteria may still retain their right to exist, as there can be a clear difference between a hysteretic and non-hysteretic contact formation of the highest peak.

While the model used for our study neglects effects, which certainly often matter in practice, such as viscoelasticity [33, 34], plasticity [35], and a roughness induced enhancement of adhesion [36, 37], occurring in systems beyond the small-slope approximation, our study substantially refines the picture having emerged from excellent, previous simulations [7, 21, 28, 38–41] addressing the origin of quasi-static, elastic adhesion hysteresis. As mentioned above, we identified the existence of several adhesion regimes instead of just two regimes. In addition, using short-range adhesion, we find the transition between high and low adhesion to be more abrupt than previous works, despite having avoided lattice trapping. This may be well the case, because we used a relative large, local Tabor parameter, which is important to properly model the approach curve [10]. Unfortunately, systematic errors only disappear with the mesh size according to $\Delta a^{1/3}$ on the approach curve [21], so that reducing them by one digit requires the use of 1,000 times the original computational resources. In multi-asperity contacts, fast convergence of non-contact traction with either decreasing Δa and/or increasing μ_{T} is also required on retraction since opposite surfaces keep "seeing" each other after a local contact broke. A new algorithm [41] appears promising regarding efficient modeling of short-range adhesion, even if it is not yet clear, how systematic errors or computational efforts scale in practice with Δa and the number of discretization elements. Nonetheless, further reducing the range of adhesion in simulations appears to be an important challenge to be met. Even more, there is conflicting evidence on what a desirable target range should be. Dispersive interactions have a range of a few Angstroms. However, analysis of experimental data lead to an estimate of 46 nm as an appropriate (effective) range of adhesion [42] in a particular system. This is still shorter ranged than what can be feasibly modeled as it comes to industrially relevant systems, as for example, in the context of valves or gecko-inspired climbing robots. Existing, systematic coarse-graining techniques certainly alleviate the situation but may have to be complemented so that they can reflect history-dependence whenever interfacial stresses are not an unambiguous function of the (mean) local interfacial separation.

Last but not least, we find that dimensionality matters in that one-dimensional and two-dimensional contacts behave differently. This is particularly apparent in the limit of single-wavelength roughness, where the saddle-point related instabilities occur in 2D but not in 1D. Randomly rough, 2D surfaces have small pull-off forces when the real contact area at pull-off is small but increase when the areas between large contact patches no longer allows for peeling. In the vicinity of the crossover between large and small adhesion, i.e., near $\tilde{\gamma} = 0.5$, randomly rough line contacts require substantially larger relative pull-off forces than 2D contacts, even if their differentials $C(q)\mathrm{d}^D q$ are similar. This means that theories that are solely based on the height spectrum as roughness information, as for example Persson's approach to adhesion [43, 44], might not be equally applicable to line and areal contacts, even if some of the discrepancies could arise due to a semi-empirical correction coefficient entering the theory. This coefficient could recently be related to the difference of the rms-height gradient averaged over the contact and that averaged over the entire surface [45]. Yet, it could also be that the theory is simply less accurate in line contacts than in areal contacts, as the theory fails to accurately account for the logarithmic corrections to the linear area-pressure relation in non-adhesive contacts at small pressures [46].

Acknowledgements

Support by the Deutsche Forschungsgemeinschaft (DFG) through grant MU 1694/5-2 is acknowledged.

Appendix

For a periodically repeated cell, the mean squares of height, height gradient, and related properties follow from sums over all $\boldsymbol{q}$ vectors having the form

$$I_n = \sum_{\boldsymbol{q}} \frac{C(q)}{A} q^n \tag{A1}$$

assuming $C(q) = A\left|\tilde{h}(q)\right|^2$ and stochastic in-plane isotropy. Specifically,

$$\overline{h}^2 = I_0,\ \overline{g}^2 = I_2,\ \ \overline{\kappa}^2 = I_4/4,\ \ v_{\text{fce}} = I_1 E^*/2 \tag{A2}$$

For a large linear system size $\mathcal{L}$, the sums can be approximated with integrals by realizing that $\Delta q = \Delta q_x = \Delta q_y = 2\pi/\mathcal{L} \to 0$ so that for the form of $C(q)$ assumed in this work,

$$\begin{aligned} I_n \ &\to\ \frac{1}{2\pi}\int \mathrm{d}q\, q\, C(q) q^n \\ &= \frac{C(q_{\mathrm{r}}) q_{\mathrm{r}}^{2+n}}{2\pi}\left[\frac{1}{2+n}\left\{1-\left(\frac{q_0}{q_{\mathrm{r}}}\right)^{2+n}\right\}+\right. \\ &\quad \left.\frac{C(q_{\mathrm{r}})}{2\pi}\frac{1}{2H-n}\left\{\left(\frac{q_s}{q_{\mathrm{r}}}\right)^{2H-n}-1\right\}\right] \end{aligned} \tag{A3}$$

The second summand in the square bracket on the right-hand side of this equation can be simplified according to

$$\lim_{n\to 2H}\frac{1}{2H-n}\left\{\left(\frac{q_s}{q_{\mathrm{r}}}\right)^{2H-n}-1\right\} = \ln\left(\frac{q_s}{q_{\mathrm{r}}}\right) \tag{A4}$$

in the special case, where $n = 2H$, e.g., for $n = 1$ and $H = 0.5$.

Thus, for the relevant range of Hurst exponents $0 < H < 1$, the ms-height is mainly due to the spectrum near q_{r} while ms-gradient and ms-curvature have their main contributions from small-wavelength undulations. The full-contact elastic energy stems predominantly from large- and small-wavelength contributions for $H < 0.5$ and $H > 0.5$, respectively.

References

[1] Dahlquist C A. *Adhesion: Fundamentals and Practice*. Nottingham (UK): MacLaren, 1966.

[2] Persson B N J. On the mechanism of adhesion in biological systems. *J Chem Phys* **118**(16): 7614 (2003)

[3] Persson B J, Albohr O, Tartaglino U, Volokitin A I, Tosatti E. On the nature of surface roughness with application to contact mechanics, sealing, rubber friction and adhesion. *J Phys: Condens Matter* **17**(1): 1–62 (2005)

[4] Joe J, Scaraggi M, Barber J R. Effect of fine-scale roughness on the tractions between contacting bodies. *Tribol Int* **111**: 52–56 (2017)

[5] Tiwari A, Wang J, Persson B N J. Adhesion paradox: Why adhesion is usually not observed for macroscopic solids. *Phys Rev E* **102**(4): 042803 (2020)

[6] Ciavarella M. Universal features in "stickiness" criteria for soft adhesion with rough surfaces. *Tribol Int* **146**: 106031 (2020)

[7] Radhakrishnan H, Akarapu S. Two-dimensional finite element analysis of elastic adhesive contact of a rough surface. *Sci Rep* **10**: 5402 (2020)

[8] Pastewka L, Robbins M O. Contact between rough surfaces and a criterion for macroscopic adhesion. *PNAS* **111**(9): 3298–3303 (2014)

[9] Joe J, Thouless M D, Barber J R. Effect of roughness on the adhesive tractions between contacting bodies. *J Mech Phys Solids* **118**: 365–373 (2018)

[10] Ciavarella M, Greenwood J, Barber J. Effect of Tabor parameter on hysteresis losses during adhesive contact. *J Mech Phys Solids* **98**: 236–244 (2017)

[11] Monti J M, Sanner A, Pastewka L. Distribution of gaps and adhesive interaction between contacting rough surfaces. *Tribol Lett* **69**: 80 (2021)

[12] Müser M H. A dimensionless measure for adhesion and effects of the range of adhesion in contacts of nominally flat surfaces. *Tribol Int* **100**: 41–47 (2016)

[13] Müser M H, Dapp W B, Bugnicourt R, Sainsot P, Lesaffre N, Lubrecht T A, Persson B N J, Harris K, Bennett A, Schulze K, et al. Meeting the contact-mechanics challenge. *Tribol Lett* **65**: 118 (2017)

[14] Persson B N J. On the fractal dimension of rough surfaces. *Tribol Lett* **54**: 99–106 (2014)

[15] Campañá C, Müser M H. Practical green's function approach to the simulation of elastic semi-infinite solids. *Phys Rev B* **74**(7): 075420 (2006)

[16] Zhou Y, Moseler M, Müser M H. Solution of boundary-element problems using the fast-inertial-relaxation-engine method. *Phys Rev B* **99**(14): 144103.1–144103.8 (2019)

[17] Dalvi S, Gujrati A, Khanal S R, Pastewka L, Dhinojwala A, Jacobs T D B. Linking energy loss in soft adhesion to surface roughness. *PNAS* **116**: 25484–25490 (2019)

[18] Hui C Y, Jagota A, Bennison S J, Londono J D. Crack blunting and the strength of soft elastic solids. *Proc Math Phys Eng* **459**: 1489–1516 (2003)

[19] Etsion I, Kligerman Y, Kadin Y. Unloading of an elastic–plastic loaded spherical contact. *Int J Solids Struct* **42**: 3716–3729 (2005)

[20] Balijepalli R G, Fischer S C, Hensel R, McMeeking R M, Arzt E. Numerical study of adhesion enhancement by composite fibrils with soft tip layers. *J Mech Phys Solids* **99**: 357–378 (2017)

[21] Wang A, Zhou Y, Müser M H. Modeling adhesive hysteresis. *Lubricants* **9**: 17 (2021)

[22] Dapp W B, Prodanov N, Müser M H. Systematic analysis of Persson's contact mechanics theory of randomly rough elastic surfaces. *J Phys-Condens Mat* **26**: 355002 (2014)

[23] Salehani M K, van Dokkum J, Irani N, Nicola L. On the load-area relation in rough adhesive contacts, *Tribol Int* **144**: 106099 (2020)

[24] Dapp W B, Müser M H. Contact mechanics of and Reynolds flow through saddle points: On the coalescence of contact patches and the leakage rate through near-critical constrictions. *EPL* **109**: 44001 (2015)

[25] Menga N, Afferrante L, Carbone G. Adhesive and adhesiveless contact mechanics of elastic layers on slightly wavy rigid substrates. *Int J Solids Struct* **88–89**: 101–109 (2016)

[26] Johnson K L. The adhesion of two elastic bodies with slightly wavy surfaces. *Int J Solids Struct* **32**(3–4): 423–430 (1995)

[27] Violano G, Afferrante L, Papangelo A, Ciavarella M. On stickiness of multiscale randomly rough surfaces. *J Adhesion* **97**: 509–527 (2019)

[28] Popov Valentin L, Li Q, Lyashenko I A, Pohrt R. Adhesion and friction in hard and soft contacts: Theory and experiment. *Friction* **9**(6): 1688–1706 (2021)

[29] Popov Valentin L, Pohrt R, Li Q. Strength of adhesive contacts: Influence of contact geometry and material gradients. *Friction* **5**(3): 308–325 (2017)

[30] Dapp W B, Lucke A, Persson B N J, Müser M H. Self-affine elastic contacts: Percolation and leakage. *Phys Rev Lett* **108**: 244301 (2012)

[31] Wang A, Müser M H. Percolation and Reynolds flow in elastic contacts of isotropic and anisotropic, randomly rough surfaces. *Tribol Lett* **69**: 1 (2020)

[32] Persson B N J, Biele J. On the stability of spinning asteroids. *Tribol Lett* **70**: 34 (2022)

[33] Tiwari A, Dorogin L, Bennett A I, Schulze K D, Sawyer W G, Tahir M, Heinrich G, Persson B N J. The effect of surface roughness and viscoelasticity on rubber adhesion. *Soft Matter* **13**: 3602–3621 (2017)

[34] Dorogin L, Tiwari A, Rotella C, Mangiagalli P, Persson B. Role of preload in adhesion of rough surfaces. *Phys Rev Lett* **118**(23): 238001 (2017)

[35] Kim J-Y, Baltazar A, Rokhlin S. Ultrasonic assessment of rough surface contact between solids from elastoplastic loading–unloading hysteresis cycle. *J Mech Phys Solids* **52**: 1911–1934 (2004)

[36] Deng W, Kesari H. Depth-dependent hysteresis in adhesive elastic contacts at large surface roughness. *Sci Rep* **9**: 1639 (2019)

[37] Guduru P. Detachment of a rigid solid from an elastic wavy surface: Theory. *J Mech Phys Solids* **55**: 445–472 (2007)

[38] Carbone G, Pierro E, Recchia G. Loading-unloading hysteresis loop of randomly rough adhesive contacts. *Phys Rev E* **92**(6): 062404 (2015)

[39] Joe J, Thouless M D, Barber J R. Effect of surface roughness on adhesive instabilities for the elastic layer. *Front Mech Eng* **6**: 61 (2020)

[40] Violano G, Afferrante L. Roughness-induced adhesive hysteresis in self-affine fractal surfaces. *Lubricants* **9**: 7 (2021)

[41] Xu Y, Zhou R X. Adhesive boundary element method using virtual crack closure technique. *Front Mech Eng* **7**: 754782 (2021)

[42] Thimons L A, Gujrati A, Sanner A, Pastewka L, Jacobs T D B. Hard-material adhesion: Which scales of roughness matter? *Exp Mech* **61**: 1109–1120 (2021)

[43] Persson B. Contact mechanics for randomly rough surfaces. *Surf Sci Rep* **61**: 201–227 (2006)

[44] Persson B N J, Scaraggi M. Theory of adhesion: Role of surface roughness. *J Chem Phys* **141**: 124701 (2014)

[45] Müser M H. Elastic contacts of randomly rough indenters with thin sheets, membranes under tension, half spaces, and beyond. *Tribol Lett* **69**(1): 25 (2021)

[46] van Dokkum J S, Salehani M K, Irani N, Nicola L. On the proportionality between area and load in line contacts. *Tribol Lett* **66**(3): 115 (2018)

Anle WANG. He received his bachelor and Ph.D. degree from Southwest Jiaotong University, China in 2011 and 2016, respectively. Since 2016 he spent his postdoctoral time in the Department of Material Science and Engineer at Saarland University. Now his research focuses on the modeling the adhesive rough contacts across multiple length scales.

Martin H. MÜSER. He received his diploma in physics from Saarland University, Germany, in 1992 and his Ph.D. degree in theoretical physics from Johannes Gutenberg University Mainz in 1995. He spent his postdoctoral time in the Department of Chemistry at Columbia University and in the Physics & Astronomy Department at the Johns Hopkins University. In 2002, he became a professor of applied mathematics at Western University in London, Ontario. After a sabbatical year at IBM, T. J. Watson, New York, he moved to Saarland University in 2009, where he held the chair of material simulations in the Department of Material Science and Technology. From 2011 to 2016, he also headed the Computational Materials Research Group at the Supercomputing Centre of Forschungszentrum Jülich. His research evolves around the simulation of thermal and mechanical properties of hard and soft-condensed matter.